

Waste heat energy harvesting using the Olsen cycle on $0.945\text{Pb}(\text{Zn}_{1/3}\text{Nb}_{2/3})\text{O}_3-0.055\text{PbTiO}_3$ single crystals

Ian M McKinley, Razmig Kandilian and Laurent Pilon

Mechanical and Aerospace Engineering Department, Henry Samueli School of Engineering and Applied Science, University of California, Los Angeles–Los Angeles, CA 90095, USA

E-mail: pilon@seas.ucla.edu

Received 9 September 2011, in final form 21 December 2011

Published 16 February 2012

Online at stacks.iop.org/SMS/21/035015

Abstract

This paper reports on direct thermal to electrical energy conversion by performing the Olsen (or Ericsson) cycle on [001]-poled $0.945\text{PbZn}_{1/3}\text{Nb}_{2/3}\text{O}_3-0.055\text{PbTiO}_3$ (PZN-5.5PT) single crystals. The cycle consists of two isothermal and two constant electric field processes. The energy density was found to decrease with increasing cycle frequency while the power density increased. The maximum energy density obtained was $150\text{ J}/1/\text{cycle}$ for temperatures between 100 and 190°C and electric field between 0 and 1.2 MV m^{-1} at frequency 0.034 Hz . The maximum power density reached 11.7 W l^{-1} at 0.1 Hz for temperatures between 100 and 190°C and electric fields between 0.2 and 1.5 MV m^{-1} . Moreover, the dielectric constant and saturation polarization of PZN-5.5PT are reported for the first time at 0.1 Hz for temperatures between 100 and 190°C . Finally, the experimental results agree relatively well with predictions by a recently developed temperature-dependent property model already validated with PMN-32PT. Inter-sample variability and sample durability are also discussed.

(Some figures may appear in colour only in the online journal)

1. Introduction

The rising interest in renewable energy and energy-efficient technologies has stimulated efforts in harvesting thermal energy that would otherwise be wasted. In 2009, an estimated 50% of the energy consumed in the United States was wasted in the form of low grade waste heat [1]. The Olsen cycle performed on pyroelectric material can convert thermal energy directly into electricity [2]. This cycle consists of two isothermal and two isoelectric field processes in the displacement versus electric field (D - E) diagram [2]. It is analogous to the Ericsson cycle, in which a working fluid undergoes two isothermal and two isobaric processes in the pressure–volume diagram [3]. Figure 1 shows the isothermal bipolar hysteresis loops at cold and hot temperatures T_{cold} and T_{hot} . It also illustrates the Olsen cycle. Process 1–2 corresponds to an increase in the electric field from E_L to E_H at constant temperature T_{cold} . Process 2–3 consists of heating the material from T_{cold} to T_{hot} under constant electric field

E_H . Process 3–4 corresponds to a decrease in the electric field from E_H to E_L at constant temperature T_{hot} . Finally, process 4–1 closes the cycle by cooling the material from T_{hot} to T_{cold} under constant electric field E_L . The area shaded in gray corresponds to the generated energy density N_D defined as the electrical energy produced per unit volume of the material per cycle. It is expressed as [2]

$$N_D = \oint E dD. \quad (1)$$

In practice, the generated energy can be harvested by delivering it to an external load or storage unit [4]. Several devices have been designed and built to implement the Olsen cycle [2, 5–11]. They have explored several heat transfer strategies ranging from laminar convective heat transfer [2, 4, 6–9] to conduction [10, 11] and nanoscale radiation [5]. The required temperature oscillations have been achieved passively in various designs [10, 12]. In order to achieve the maximum device performance, it is also necessary to identify

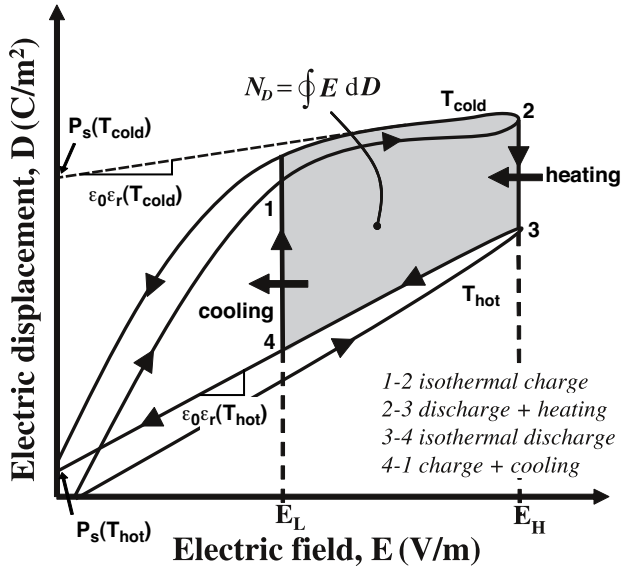


Figure 1. Electric displacement versus electric field for a typical pyroelectric material at temperatures T_{hot} and T_{cold} along with the Olsen cycle. The electrical energy generated per cycle is represented by the gray area enclosed by 1–4.

the best pyroelectric material and the associated optimum operating temperature range.

The present study aims to assess the energy harvesting performance of commercially available [001]-poled $0.945\text{PbZn}_{1/3}\text{Nb}_{2/3}\text{O}_3-0.055\text{PbTiO}_3$ (PZN-5.5PT) single crystals undergoing the Olsen cycle. Particular attention was paid to the effects of temperature, electric field and cycle frequency as well as inter-sample variability. Other objectives of this study were to measure the dielectric properties of PZN-5.5PT at low frequencies and to validate a recently developed physics-based model [13].

2. Background

2.1. PZN-PT properties

The properties of PZN-PT have been studied extensively as it is a popular ferroelectric material used in sensors and actuators [14–23]. Poled single crystal PZN-4.5PT undergoes a phase transformation sequence from rhombohedral (R) to tetragonal (T) to cubic (C) during heating from 25 to 160 °C under zero electric field [19]. A small fraction of rhombohedral domains exist in the tetragonal phase [19]. The phase diagram for PZN- x PT indicates that, for PZN-5.5PT, the rhombohedral to tetragonal transition occurs between 122 and 130 °C and the tetragonal to cubic transition occurs around $T_{Curie} = 165$ °C [20]. Renault *et al* [23] showed that during field cooling from 177 to 27 °C [001]-oriented PZN-4.5PT has an additional orthorhombic (O) phase and undergoes a C–T–O–R phase transition sequence. The authors also demonstrated that the transition temperatures were dependent on the applied electric field which varied from 0 to 0.3 MV m⁻¹.

Ren *et al* [14] showed that electric-field-induced phase transitions and piezoelectric properties of PZN- x PT are strongly dependent on temperature and composition for x between 4.5 and 8%. In addition, Shen and Cao [17] reported the temperature dependence of the piezoelectric, pyroelectric and dielectric properties of PZN- x PT poled by two different methods for x equal to 4.5 and 8%. The relative permittivity and saturation polarization of PZN-4.5PT were found to be extremely sensitive to (i) the applied electric field used during poling [22] and (ii) to the poling method [17]. Although the properties of PZN-4.5PT have been reported in the literature [14–23], to the best of our knowledge, dielectric properties of PZN-5.5PT, investigated here, have not been reported.

2.2. Olsen cycle on PZN-PT

Khodayari *et al* [24] studied the energy harvesting capabilities of [110]-oriented PZN-4.5PT using the Olsen cycle. The authors achieved 216.5 J/1/cycle (1 J/1/cycle = 1 mJ/cm³/cycle) by successively dipping a 1 mm thick single crystal PZN-4.5PT sample in baths at 100 and 160 °C while the electric fields varied between $E_L = 0$ MV m⁻¹ and $E_H = 2$ MV m⁻¹. Zhu *et al* [25] also used 1.1 mm thick [110]-oriented PZN-4.5PT single crystals to examine the energy generated with electric-field-induced phase transitions through rhombohedral, orthorhombic and tetragonal phases during the Olsen cycle. The authors obtained 101.8 J/1/cycle operating between temperatures 100 and 130 °C and electric fields $E_L = 0$ MV m⁻¹ and $E_H = 2$ MV m⁻¹ [25]. For these operating conditions, they determined that, during the isothermal processes 1–2 and 3–4 in the Olsen cycle, the samples experienced rhombohedral to orthorhombic (R–O) and orthorhombic to tetragonal (O–T) frequency-dependent phase transitions, respectively. Zhu *et al* [25] also found that the energy density increased with reducing the duration of isothermal process 1–2 and increasing the duration of isothermal process 3–4 which varied from 0.1 to 100 s. Finally, if the isothermal processes were of equal duration, the energy density increased with increasing duration [25]. In both of these studies [24, 25], it is unclear if these experimental results were averaged over multiple cycles and/or were repeated for different samples. In contrast, the present study performs the Olsen cycle on several PZN-5.5PT single crystal samples and assesses the sample variability in terms of generated energy.

2.3. Modeling

Recently, Kandilian *et al* [13] derived a model estimating the energy harvesting capabilities of single crystal relaxor ferroelectric materials undergoing the Olsen cycle. The model expresses the energy density as [13]

$$N_D = (E_H - E_L) \left\{ \frac{\epsilon_0}{2} [\epsilon_r(T_{cold}) - \epsilon_r(T_{hot})] (E_H + E_L) + \left[P_s(T_{cold}) - P_s(T_{hot}) + \frac{d_{33}x_3}{s_{33}} \right] \right\} \quad (2)$$

where ε_0 is the vacuum permittivity ($=8.854 \times 10^{-12} \text{ F m}^{-1}$), $\varepsilon_r(T_{\text{cold}})$ and $\varepsilon_r(T_{\text{hot}})$ are the low frequency ($\sim 0.1 \text{ Hz}$) relative permittivities of the pyroelectric material at the cold and hot operating temperatures T_{cold} and T_{hot} , respectively. The saturation polarizations of the pyroelectric material at T_{cold} and T_{hot} are respectively denoted by $P_s(T_{\text{cold}})$ and $P_s(T_{\text{hot}})$ and expressed in C m^{-2} [26]. In addition, d_{33} is the piezoelectric coefficient of the single crystal (in C N^{-1}), s_{33} is the elastic compliance of the single crystal (in $\text{m}^2 \text{ N}^{-1}$) and $x_3 = \alpha_3(T_{\text{hot}} - T_{\text{cold}})$, where α_3 is the thermal expansion coefficient (in K^{-1}). Note that this model was based on the assumption that the dielectric contribution to the primary pyroelectric coefficient was negligible compared with the dipole contribution (see equation (8) in [13]). This model was validated against experimental data collected on PMN-32PT single crystals and using properties reported in the literature [27–30] for $T_{\text{cold}} = 80^\circ\text{C}$ and T_{hot} varying from 130 to 170 $^\circ\text{C}$, while E_L was 0.2 MV m^{-1} and E_H ranged from 0.4 to 0.9 MV m^{-1} [13]. The model given by equation (2) is expressed as a function of material properties typically reported in the literature. Thus, it can enable rapid identification of promising materials for waste heat harvesting without physically performing the Olsen cycle.

The present paper aims (i) to assess the performance of PZN-5.5PT single crystals in converting waste heat into electricity, (ii) to measure their dielectric properties and (iii) to further validate the above model.

3. Experiments

3.1. Samples

In the present study, five single crystal PZN-5.5PT samples were purchased from Microfine Materials Technologies Pte Ltd, Singapore. The samples were poled in the [001] direction. Their surface area and thickness were $1 \times 1 \text{ cm}^2$ and 200 μm , respectively. Each $1 \times 1 \text{ cm}^2$ face of the samples was coated with a $\sim 10 \text{ nm}$ NiCr bond layer and a $\sim 1 \mu\text{m}$ thick $\text{Au}_{0.68}\text{Pd}_{0.32}$ electrode. These layers were deposited by an RF sputter-deposition technique. Electrical wires were attached to the electrodes using conductive silver epoxy.

3.2. D – E loops

Isothermal bipolar displacement versus electric field hysteresis curves were collected at various temperatures by applying a triangular voltage with frequency of 0.1 Hz across the single crystal samples. The samples were placed in a silicone oil bath at the desired temperatures of 100, 125, 150, 175 or 190 $^\circ\text{C}$. The amplitude of the voltage corresponded to an electric field varying from -1 to 1 MV m^{-1} . All measurements were repeated five times on each of the five different samples to assess repeatability and experimental uncertainty.

Moreover, the saturation polarization $P_s(T)$ and the dielectric constant $\varepsilon_r(T)$ of each sample at temperature T were evaluated by linearly fitting the section of the bipolar

D – E loops corresponding to a relatively large electric field decreasing from 1 to 0.5 MV m^{-1} according to [31]

$$D(E, T) = \varepsilon_0 \varepsilon_r(T) E + P_s(T). \quad (3)$$

The saturation polarization $P_s(T)$ is equal to the electric displacement in the linear fit of D versus E extrapolated at zero electric field [28] and the slope of this linear fit corresponds to the product $\varepsilon_0 \varepsilon_r(T)$ as illustrated in figure 1.

Moreover, isothermal unipolar D – E loops were collected on sample 5 for the same above temperatures. They were compared with bipolar D – E loops along with the associated values of $\varepsilon_r(T)$ and $P_s(T)$.

3.3. Olsen cycle

The Olsen cycle was performed on the PZN-5.5PT samples for (i) different values of low and high electric fields E_L and E_H , (ii) various hot operating temperature T_{hot} and (iii) various cycle frequency f . The experimental set-up consisted of a thermal and an electrical subsystem. The experimental apparatus and procedure were identical to those used in our previous studies [13, 32] and need not be repeated. The cold operating temperature T_{cold} was fixed at 100 $^\circ\text{C}$. The hot operating temperature was varied from 125 to 190 $^\circ\text{C}$. The electric fields E_L and E_H ranged from 0 to 0.2 MV m^{-1} and from 0.5 to 1.5 MV m^{-1} , respectively. The overall cycle frequency was defined as $f = (\tau_{12} + \tau_{23} + \tau_{34} + \tau_{41})^{-1}$, where τ_{ij} corresponds to the duration of process i – j . It varied from 0.021 to 0.15 Hz by changing the duration of the isoelectric field heating and cooling processes 2–3 and 4–1, denoted by τ_{23} and τ_{41} (figure 1). However, the time rate of change of the electric field during the isothermal processes 1–2 and 3–4 remained the same at 0.4 $\text{MV m}^{-1} \text{ s}^{-1}$. Note that this rate was identical to that used to collect the D – E loops between -1 and 1 MV m^{-1} at 0.1 Hz. In other words, τ_{12} and τ_{34} were equal and constant for a given electric field span. For example, $\tau_{12} = \tau_{34} = 2.5 \text{ s}$ for $E_H - E_L = 1 \text{ MV m}^{-1}$. The times τ_{23} and τ_{41} varied between 0.5 and 20 s corresponding to the cycle frequency varying from 0.15 to 0.021 Hz.

The energy density generated per cycle N_D (expressed in J/cycle) is represented by the area enclosed by the cycle in the D – E diagram (figure 1). It was calculated by numerical integration of equation (1) using the trapezoidal rule. In addition, the power density P_D is the amount of energy generated by the pyroelectric material per unit volume per unit time and is expressed in W l^{-1} . It is defined as $P_D = N_D f$, where f is the Olsen cycle frequency.

4. Results and discussion

4.1. D – E loops

Figure 2 shows typical isothermal bipolar D – E loops at $T_{\text{cold}} = 100^\circ\text{C}$ as well as loops for T_{hot} equal to (a) 125 $^\circ\text{C}$, (b) 150 $^\circ\text{C}$, (c) 175 $^\circ\text{C}$ and (d) 190 $^\circ\text{C}$ obtained with sample 5. The isothermal D – E loops followed a counter-clockwise path. Figure 2 also shows that Olsen cycles corresponding to the above temperatures with $E_L = 0.0$ or 0.2 MV m^{-1} and $E_H =$

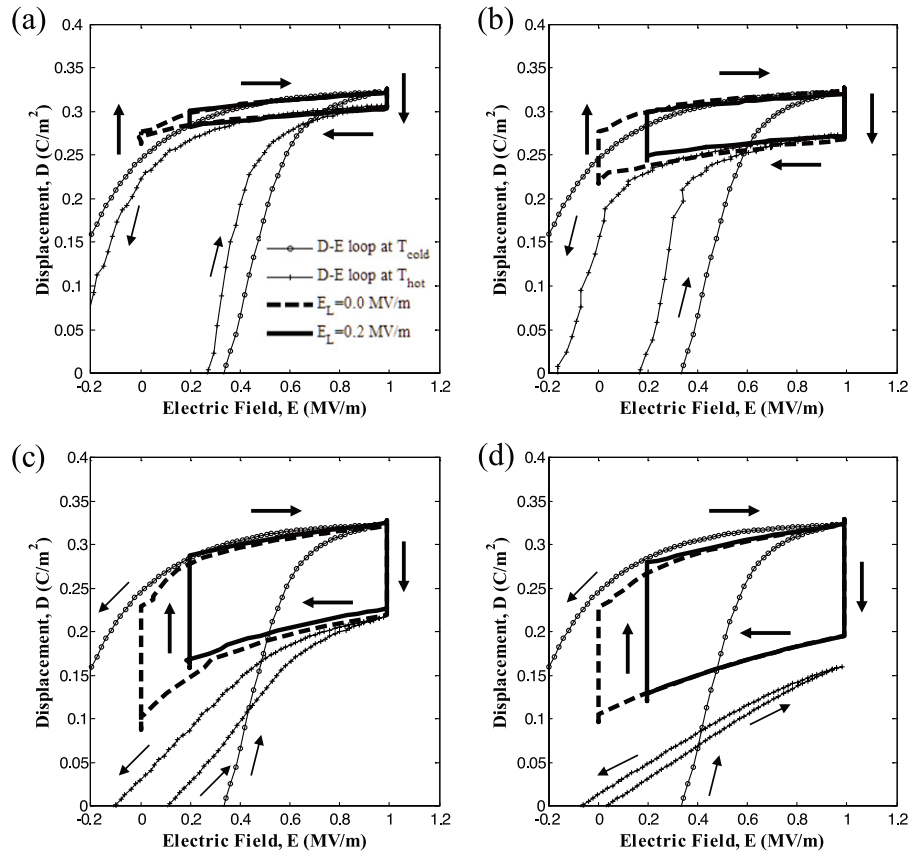


Figure 2. Isothermal bipolar D - E loops and experimental Olsen cycles at $E_L = 0.0$ and 0.2 MV m^{-1} for PZN-5.5PT (sample 5) with $T_{\text{cold}} = 100^\circ\text{C}$ and $E_H = 1.0 \text{ MV m}^{-1}$ for T_{hot} equal to (a) 125°C , (b) 150°C , (c) 175°C and (d) 190°C .

Table 1. Saturation polarization $P_s(T)$ and dielectric constant $\epsilon_r(T)$ for the five [001] PZN-5.5PT samples used in this study.

Sample	Properties	Units					
	T	($^\circ\text{C}$)	100	125	150	175	190
1	$P_s(T)$	(C m^{-2})	0.233	0.221	0.2049	0.0593	—
	$\epsilon_r(T)$	—	2535	4327	4833	16 684	—
2	$P_s(T)$	(C m^{-2})	0.2554	0.2569	0.2322	0.0959	0.034
	$\epsilon_r(T)$	—	2937	3445	4352	13 889	12 781
3	$P_s(T)$	(C m^{-2})	0.2078	0.2110	0.2222	0.1346	0.0529
	$\epsilon_r(T)$	—	3617	5620	5136	10 015	13 598
4	$P_s(T)$	(C m^{-2})	0.2922	0.2801	0.2458	0.1308	0.0451
	$\epsilon_r(T)$	—	3500	3471	3840	10 448	14 364
5	$P_s(T)$	(C m^{-2})	0.2967	0.2814	0.2397	0.1266	0.0384
	$\epsilon_r(T)$	—	3180	3180	4100	11 100	14 500

1.0 MV m^{-1} . Results indicated that all [001] PZN-5.5PT samples were ferroelectric at 100, 125 and 150°C . They were paraelectric at 190°C as their saturation polarization vanished (figure 2(d)). In addition, samples 1 and 2 were paraelectric at 175°C while samples 3, 4 and 5 were ferroelectric at 175°C .

Moreover, table 1 summarizes the values of $P_s(T)$ and $\epsilon_r(T)$ retrieved from the isothermal D - E loops for each sample at different temperatures. The greatest inter-sample variability in D - E loops and in the resulting $P_s(T)$ and $\epsilon_r(T)$ values was observed at 125 and 175°C . The relative errors in $P_s(T)$ and $\epsilon_r(T)$ among samples were less than 20% for temperatures 100, 150 and 190°C . They were less than 25% and 30% for temperatures 125 and 175°C , respectively. The

variability at 125°C can be attributed to the presence of mixed rhombohedral and tetragonal phases. In fact, the volume ratio of these phases may vary from one sample to another due to small chemical inhomogeneities [33]. The sample variability observed at 175°C can be attributed to the fact that samples 3, 4 and 5 were ferroelectric with $P_s \approx 0.13 \text{ C m}^{-2}$ while samples 1 and 2 were paraelectric at this temperature.

Finally, figure 3 compares unipolar and bipolar D - E loops performed on sample 5 at 100°C . The unipolar D - E loop, corresponding to a frequency of 0.2 Hz, had the same time rate of change in the electric field as the bipolar D - E loop measured at 0.1 Hz. Note also that the unipolar D - E loops measured at 0.1 and 0.2 Hz were nearly identical.

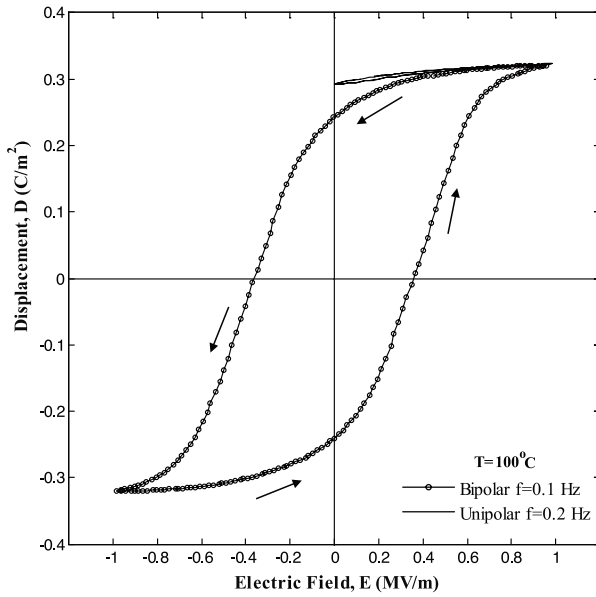


Figure 3. Isothermal bipolar D - E loops at 0.1 Hz and unipolar D - E loops at 0.2 Hz for PZN-5.5PT (sample 5) at $T = 100^\circ\text{C}$.

A notable difference between the unipolar and bipolar D - E loops at 100°C was the absence of a field-induced phase transition in the unipolar loops. Such a phase transition was responsible for the nonlinear behavior of the bipolar D - E loops at low electric field. In contrast, the unipolar D - E loops followed a nearly linear path between 0.0 and 1.0 MV m^{-1} . Figure 3 establishes that the unipolar D - E loops followed the upper curve of the bipolar D - E loop corresponding to a decreasing electric field. Thus, analysis of the unipolar D - E loops or the upper curve of bipolar D - E loops resulted in nearly identical values of saturation polarization $P_s(T)$ and dielectric permittivity $\epsilon_0\epsilon_r(T)$. The same conclusions were reached at other temperatures (not shown). Finally, the D - E loops were closed for all temperatures indicating that there was no leakage current.

4.2. Effect of frequency on N_D and P_D

Figure 4 shows the isothermal bipolar D - E loops at temperatures 100 and 190°C for sample 4. It also depicts the experimental Olsen cycle in the D - E diagram for sample 4 at various cycle frequencies between 0.021 and 0.15 Hz. The cycle followed a clockwise path and was performed between $T_{\text{cold}} = 100^\circ\text{C}$ and $T_{\text{hot}} = 190^\circ\text{C}$ and electric field from $E_L = 0\text{ MV m}^{-1}$ to $E_H = 1.0\text{ MV m}^{-1}$. Note also that all the experimental Olsen cycles were closed and, unlike P(VDF-TrFE) [32], no leakage current was observed.

First, it is interesting to note that the Olsen cycles measured at frequencies of 0.021 and 0.034 Hz overlapped. Indeed, for these frequencies, the electric displacement had reached steady state, i.e. $\partial D/\partial t = 0$, before the electric field was varied. In this case, processes 1-2 and 3-4 followed a relatively smooth path, indicating that the four different processes in the Olsen cycle were performed under quasi-equilibrium conditions.

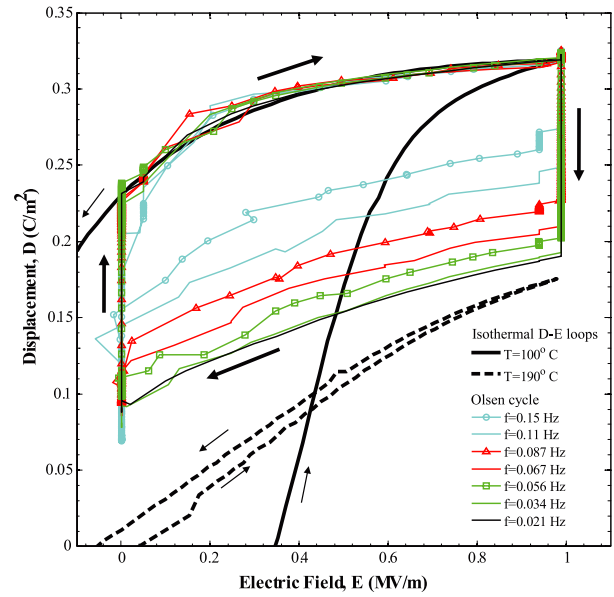


Figure 4. D - E diagram of isothermal bipolar D - E loops and experimental Olsen cycles at various frequencies for PZN-5.5PT (sample 4). The temperatures T_{cold} and T_{hot} were maintained at 100 and 190°C , respectively, and the low and high electric fields E_L and E_H were set at 0.0 and 1.0 MV m^{-1} , respectively.

Moreover, for cycle frequencies larger than 0.034 Hz, the isoelectric field processes 2-3 and 4-1 were not performed under quasi-equilibrium conditions. For such cycle frequencies, the electric displacement had not reached steady state before the electric field was varied to perform processes 1-2 and 3-4. In other words, the phase transition was incomplete. In addition, the Olsen cycles did not follow a smooth path between E_L and E_H during processes 1-2 and 3-4 in the D - E diagram, as illustrated in figure 4.

Figures 5(a) and (b) respectively show the energy density and power density as functions of frequency for the Olsen cycles performed on sample 4 and reported in figure 4. Each data point corresponds to the energy density or power density averaged over five cycles. The associated error bars correspond to two standard deviations or a 95% confidence interval. The energy density reached a plateau of 140 J/cycle at frequencies below 0.034 Hz and decreased with increasing cycle frequency. Reducing the cycle frequency below 0.034 Hz, by increasing the duration of the isoelectric field processes 2-3 and 4-1, did not result in larger energy density because each process of the Olsen cycle was performed under quasi-equilibrium.

Conversely, the power density increased with increasing frequency and reached a maximum of 10.1 W l^{-1} at 0.1 Hz. For frequencies larger than 0.1 Hz, P_D decreased with increasing frequency. This can be explained by considering the expression $P_D = N_D(f)f$. For frequencies less than 0.1 Hz, the decrease in $N_D(f)$, previously discussed, was compensated by the increase in frequency so that P_D increased. However, beyond 0.1 Hz, N_D decreased significantly with frequency, resulting in smaller values of P_D . In practice, the operating frequency could be adjusted according to the power needed for a given load. Note that the frequency of 0.15 Hz

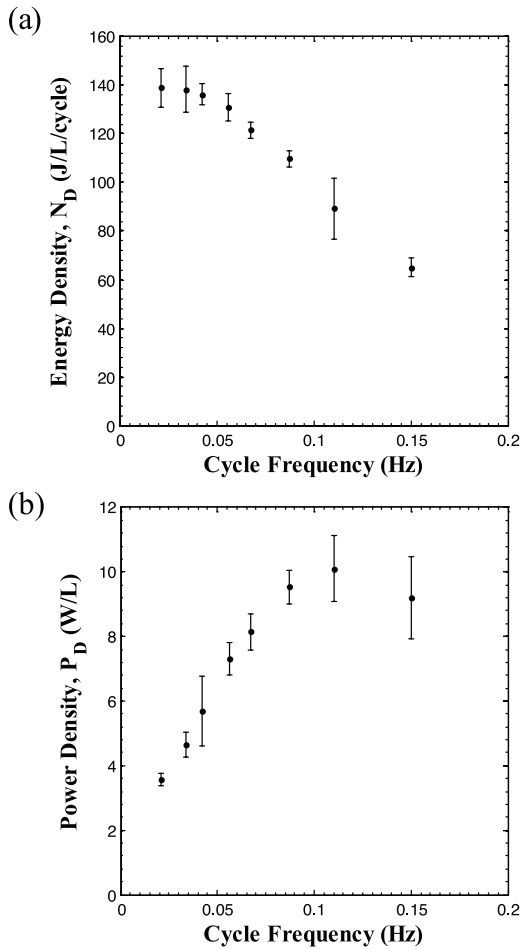


Figure 5. Experimentally measured (a) energy density and (b) power density generated with PZN-5.5PT single crystal (sample 4) as a function of cycle frequency. The temperatures T_{cold} and T_{hot} were maintained at 100 and 190 °C, respectively. The low and high electric fields E_L and E_H were set at 0.0 and 1.0 MV m⁻¹, respectively.

corresponded to $\tau_{23} = \tau_{41} = 0.5$ s while the time required to physically transfer the sample between the hot and cold baths was ~ 0.25 s per transfer.

Furthermore, the Biot number for the pyroelectric assembly (film with electrodes) is defined as $Bi = hb/k_{\text{eff}}$, where h is the heat transfer coefficient, and b and k_{eff} are the sample thickness and effective thermal conductivity, respectively. The heat transfer coefficient $h = 300$ W m⁻² K⁻¹ corresponded to convective quenching in an oil bath [34]. The effective thermal conductivity of the assembly was estimated using the series model. The thermal conductivity of PZN-5.5PT could not be found in the literature and was approximated to be that of PZT, i.e., $k \simeq 1.2$ W m⁻¹ K⁻¹ at room temperature [35] while that of gold was $k = 310$ W m⁻¹ K⁻¹ [36]. Thus, the effective thermal conductivity of the assembly of thickness $b = 202$ μm was $k_{\text{eff}} \simeq 1.21$ W m⁻¹ K⁻¹ resulting in $Bi \simeq 0.05$ or $Bi \ll 1$. Therefore, the temperature was uniform across the sample and the lumped capacitance approximation was valid for all conditions considered [36].

Finally, the thermal time constant τ associated with processes 2–3 and 3–4 can be estimated as $\tau = \rho_{\text{eff}}c_{p,\text{eff}}b/h$ [36], where ρ_{eff} and $c_{p,\text{eff}}$ are the effective density and specific heat of the pyroelectric assembly, respectively. The thermal time constant was estimated to be 1.68 s for a 200 μm thick PZN-5.5PT film with $\rho = 8000$ kg m⁻³ [37] and $c_p = 312.5$ J kg⁻¹ K⁻¹ [38] sandwiched between two 1 μm thick Au_{0.68}Pd_{0.32} electrodes having $\rho = 16951$ kg m⁻³ [39] and specific heat $c_p = 156.8$ J kg⁻¹ K⁻¹. This time constant indicates that for cycle frequencies above 0.065 Hz the sample may have not reached thermal equilibrium during processes 2–3 and 4–1 of the Olsen cycle.

4.3. Sample variability at peak power

For practical purposes and for validating the model, it is important to assess sample variability. Figure 6 shows the power density generated experimentally as a function of high electric field E_H at cycle frequency of 0.1 Hz for four different samples. Here also, each data point corresponds to the power density averaged over five cycles and the associated error bars correspond to two standard deviations. In these cycles, T_{cold} and E_L were set to be 100 °C and 0.2 MV m⁻¹, respectively. The temperature T_{hot} varied from 125 to 190 °C while E_H ranged from 0.5 to 1.5 MV m⁻¹. Figure 6 demonstrates that, for all samples, the power density increases with increasing electric field E_H and with hot source temperature T_{hot} . The maximum power obtained was 11.7 W l⁻¹ for $T_{\text{cold}} = 100$ °C, $T_{\text{hot}} = 190$ °C, $E_L = 0.2$ MV m⁻¹ and $E_H = 1.5$ MV m⁻¹. Increasing the electric field E_H beyond 1.5 MV m⁻¹ during the Olsen cycle led to sample failure caused by excessive thermo-electro-mechanical stress.

Furthermore, the maximum relative error in P_D among samples for all values of E_H was 18.3% for $T_{\text{hot}} = 125$ °C. It decreased to 18.0%, 9.8%, and 6.5% as T_{hot} increased from 150, 175 to 190 °C, respectively. The larger variability observed at lower temperature can be attributed to the large differences in the rhombohedral and tetragonal volume fractions among samples. This was already observed in the bipolar D – E loops and in the retrieved properties $P_s(T)$ and $\epsilon_r(T)$. On the other hand, the value of E_H was found to have no significant effect on sample variability.

4.4. Energy density under quasi-equilibrium conditions

Figures 7 and 8 show the generated energy density N_D as a function of electric field E_H for sample 5 with low electric field E_L equal to 0.0 and 0.2 MV m⁻¹, respectively. In all cases, the temperature T_{cold} was 100 °C while T_{hot} was (a) 125, (b) 150, (c) 175 and (d) 190 °C. The cycle frequency was 0.034 Hz corresponding to Olsen cycles with quasi-equilibrium processes, as previously discussed. Results for $E_H = 1.0$ MV m⁻¹ correspond to the Olsen cycles shown in figure 2 for each value of T_{hot} .

Figures 7 and 8 indicate that the energy density increased with increasing values of T_{hot} and E_H . They demonstrate that operating the cycle with T_{hot} above $T_{\text{Curie}} = 165$ °C yields significantly higher energy densities than cycles

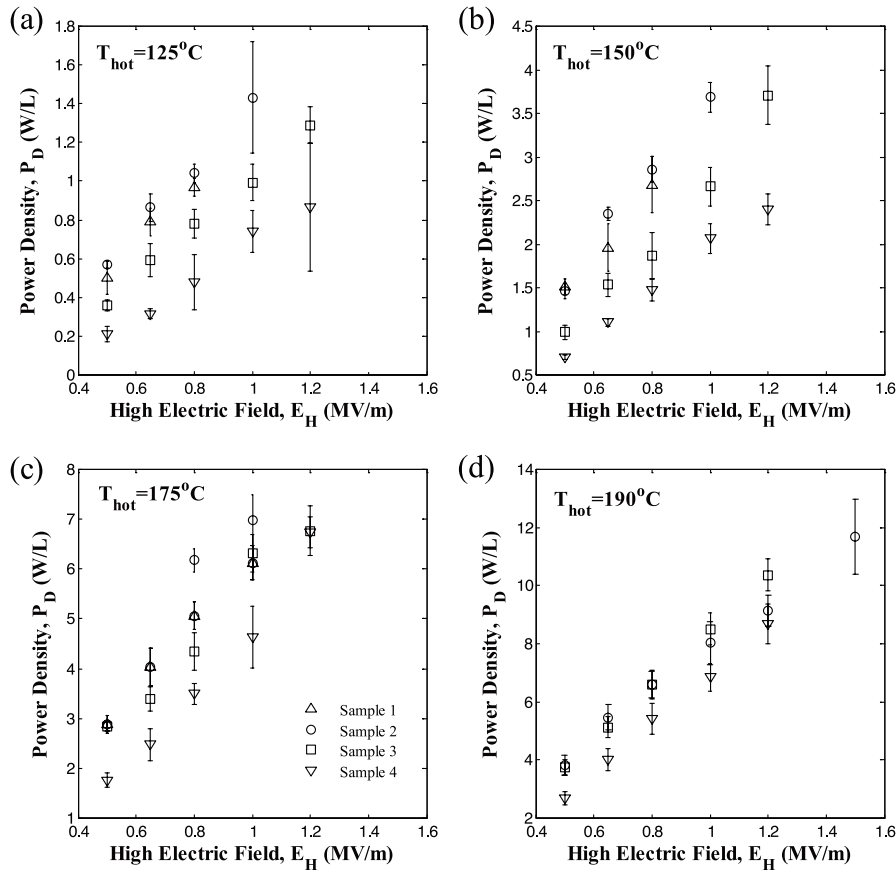


Figure 6. Experimentally measured power density generated at 0.1 Hz from four different samples of PZN-5.5PT single crystal as a function of high electric field E_H for T_{hot} equal to (a) 125 °C, (b) 150 °C, (c) 175 °C and (d) 190 °C. The temperature T_{cold} was maintained at 100 °C and the low electric field E_L was set at 0.2 MV m⁻¹.

operating below T_{Curie} . In fact, a maximum energy density of 150 J/1/cycle was achieved for operating temperatures between $T_{\text{cold}} = 100$ °C and $T_{\text{hot}} = 190$ °C and electric fields E_L and E_H equal to 0.0 and 1.2 MV m⁻¹, respectively.

In addition, increasing E_L resulted in a decrease in the generated energy density. For example, the maximum energy density decreased from 150 to 124 J/1/cycle as E_L increased from 0.0 to 0.2 MV m⁻¹ for the same $T_{\text{cold}} = 100$ °C, $T_{\text{hot}} = 190$ °C and $E_H = 1.2$ MV m⁻¹. This indicates that the PZN-5.5PT sample did not become depoled when lowering the applied electric field to 0.0 MV m⁻¹, unlike observations made with PMN-32PT [13]. Since PZN-5.5PT retains its polarization at zero electric field, the isoelectric field cooling process 4–1 can be performed at $E_L = 0$ MV m⁻¹ which may simplify the practical implementation of the Olsen cycle.

Moreover, it is interesting to compare the maximum energy density of 150 J/1/cycle obtained with PZN-5.5PT with 100 J/1/cycle obtained with PMN-32PT for the same temperature difference (90 °C) and for E_L and E_H equal to 0.2 and 0.9 MV m⁻¹, respectively. However, note that T_{cold} and T_{hot} were 80 and 170 °C for PMN-32PT [13] instead of 100 and 190 °C for PZN-5.5PT. This suggests that these two materials should be operated in slightly different temperature ranges for optimum performance. This could be useful in a multistage pyroelectric converter as envisioned by Olsen *et al* [9]. Another material that could be included in the same

multistage device is [110]-oriented PZN-4.5PT whose Curie temperature is around 157 °C [20] compared with 150 °C and 165 °C for PMN-32PT and PZN-5.5PT, respectively.

Finally, Khodayari *et al* [24] obtained 216.5 J l⁻¹ with PZN-4.5PT single crystal samples with operating conditions T_{cold} , T_{hot} , E_L and E_H equal to 100 °C, 160 °C, 0.0 MV m⁻¹ and 2.0 MV m⁻¹, respectively. The larger energy density obtained for PZN-4.5PT can be attributed to the larger electric field span ($E_H - E_L$) and to the lower Curie temperature. Indeed, the lower Curie temperature of PZN-4.5PT allowed for the tetragonal to cubic phase transition to occur for smaller temperature swing but with the same value of T_{cold} . This results in reduced thermal stress on the samples. It may also be why the PZN-4.5PT samples were able to withstand electric fields as high as 2.0 MV m⁻¹ without sample failure [24, 25] compared with up to 1.5 MV m⁻¹ in the present study.

4.5. Model predictions

Figures 7 and 8 also compare experimental energy density generated by sample 5 with predictions of the model given by equation (2). The saturation polarization and dielectric constant of sample 5 at T_{cold} and T_{hot} retrieved from D – E loops are given in table 1. Here, the last term of equation (2), corresponding to the contribution of thermal expansion to the energy density, was ignored. Indeed, the Olsen cycles

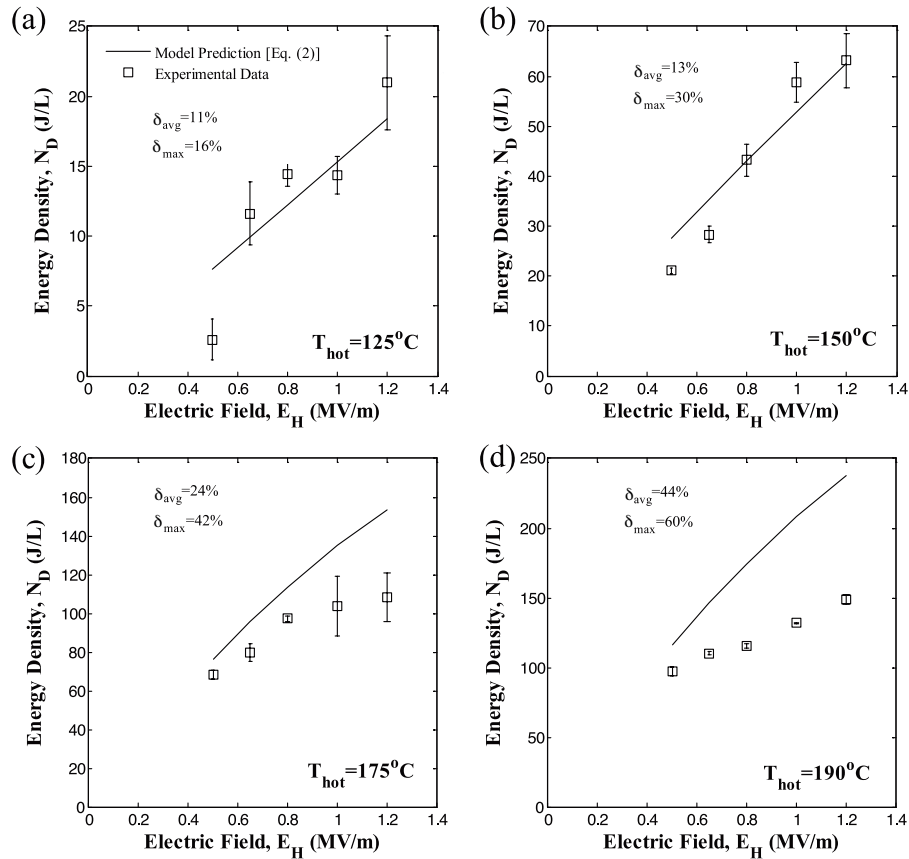


Figure 7. Experimentally measured energy density generated at 0.034 Hz from PZN-5.5PT single crystal (sample 5) versus high electric field E_H for T_{hot} equal to (a) 125 °C, (b) 150 °C, (c) 175 °C and (d) 190 °C. The temperature T_{cold} was maintained at 100 °C and the low electric field E_L was set at 0.0 MV m⁻¹. The solid line corresponds to predictions by equation (2) using properties retrieved from isothermal D - E loops (table 1).

performed on PZN-5.5PT fell on or within the bounds of the isothermal D - E loops at T_{cold} and T_{hot} (figure 2), indicating that thermal expansion did not contribute to the generated energy.

Figures 7 and 8 also report the average and maximum relative error between experimental data and model predictions denoted by δ_{avg} and δ_{max} , respectively. Relatively good agreement was observed between model predictions and experimental data, particularly for temperature T_{hot} less than 175 °C and $E_L = 0.2$ MV m⁻¹. Then, the average relative error was less than 24%. Both the average and maximum relative errors were larger for $E_L = 0.0$ MV m⁻¹ than for $E_L = 0.2$ MV m⁻¹ for any given temperature T_{hot} . This can be explained by considering the isothermal D - E loops shown in figures 2 and 3. For low electric fields ($E < 0.2$ MV m⁻¹) and for temperatures below $T_{Curie} = 165$ °C, the material is ferroelectric and the electric displacement is a nonlinear function of the electric field. This nonlinearity was also observed by Zhu *et al* [25] for [110]-oriented PZN-4.5PT and was attributed to electric-field-induced phase transitions. This phenomenon was not accounted for by the above model which treated $\epsilon_r(T)$ as a function of temperature only [13]. However, $\epsilon_r(T)$ could be assumed to depend only on T for electric fields larger than 0.2 MV m⁻¹ as previously discussed.

Moreover, figures 7(d) and 8(d) indicate that the average difference between experimental and model predictions

reached 44 and 33% for $E_L = 0.0$ and 0.2 MV m⁻¹ at $T_{hot} = 190$ °C, respectively. For such a large value of T_{hot} , the model systematically overpredicted the experimental data. For $T_{hot} = 175$ °C, the discrepancies can be attributed to the fact that the quasi-equilibrium Olsen cycles did not follow the isothermal D - E loop as the electric field was reduced from 1 to 0 MV m⁻¹ (process 3-4) as illustrated in figure 2(c). This suggests that the sample did not undergo the same phase transition during the isothermal D - E loops and the Olsen cycle. However, for $T_{hot} = 190$ °C process 2-3 of the Olsen cycles did not span the same electric displacement as the isothermal D - E loop as illustrated in figure 2(d). An electric displacement extending beyond the bounds of the D - E loops was attributed to positive thermal expansion by Kandilian *et al* [13]. Conversely, the reduced electric displacement span can be attributed to negative thermal expansion. The lattice parameters of PZN-5.5PT were reported to be constant between 190 and 100 °C [18] indicating zero thermal expansion, whereas the thermal expansion coefficient of Au_{0.75}Pd_{0.25} was reported to be 12 $\mu\text{m m}^{-1} \text{K}^{-1}$ [39]. The mismatch in thermal expansion coefficients between the electrode and the PZN-5.5PT sample induced a tensile stress in the material, which may have resulted in a decrease in sample thickness. This phenomenon was not observed for $T_{hot} = 125$ and 150 °C as is evident in figures 2(a) and (b) where the Olsen cycles tended to follow the path of the unipolar D - E loops measured

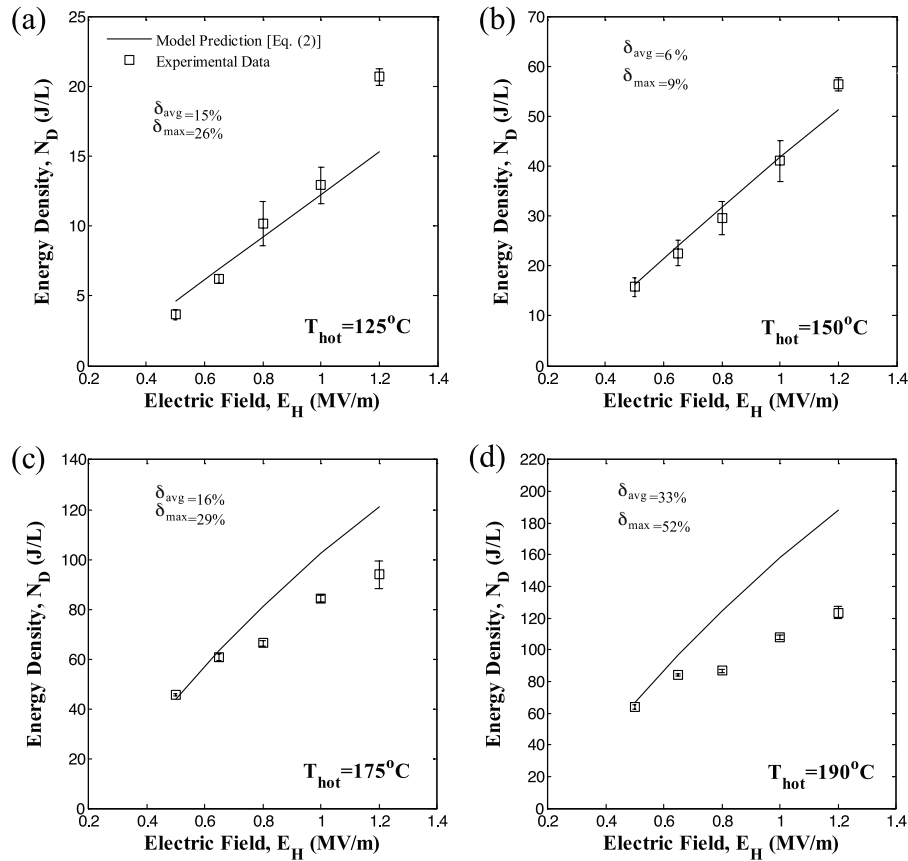


Figure 8. Experimentally measured energy density generated at 0.034 Hz from PZN-5.5PT single crystal (sample 5) versus high electric field E_H for T_{hot} equal to (a) 125°C , (b) 150°C , (c) 175°C and (d) 190°C . The temperature T_{cold} was maintained at 100°C and the low electric field E_L was set at 0.2 MV m^{-1} . The solid line corresponds to predictions by equation (2) using properties retrieved from isothermal D - E loops (table 1).

at T_{hot} . Then, good agreement was observed between model predictions and experimental data.

4.6. Sample durability

The samples used in this study broke after 100–250 cycles. The successive thermal stress in combination with the electrically induced strains contributed to the samples eventually cracking and breaking. This explains why data were not reported for all samples under all conditions (figure 6). Strategies to increase the sample durability include (i) pre-stressing the sample such as in thin layer unimorph ferroelectric driver and sensor actuators [40] and (ii) applying a conformal coating (e.g. Parylene HT) to the sample [41].

5. Conclusion

This study presented experimental measurements of energy and power densities generated by performing the Olsen cycle on [001]-poled PZN-5.5PT single crystals. It showed that, as the cycle frequency increased, the energy density decreased while the power density increased up to 0.1 Hz when it reached a peak. For temperatures $T_{cold} = 100^\circ\text{C}$ and $T_{hot} = 190^\circ\text{C}$ and electric fields between 0.2 and 1.5 MV m^{-1} the power densities reached a maximum of 11.7 W l^{-1} at 0.1 Hz. The maximum energy density achieved was 150 J l^{-1}

at frequency 0.034 Hz for $T_{cold} = 100^\circ\text{C}$, $T_{hot} = 190^\circ\text{C}$, $E_L = 0.0\text{ MV m}^{-1}$ and $E_H = 1.2\text{ MV m}^{-1}$. Sample variability was relatively small. It was the largest around 125°C due to variation in the rhombohedral/tetragonal volume fraction among samples and around 175°C due to differences in Curie temperature. Moreover, the dielectric constant and saturation polarization of PZN-5.5PT are presented in table 1 for temperatures between 100 and 190°C at 0.1 Hz. Finally, the results confirmed the validity of a recently developed model [13] given by equation (2) predicting the energy density generated from ferroelectric single crystals using the Olsen cycle under quasi-equilibrium conditions.

Acknowledgments

This research has been supported in part by NSF-IGERT program Clean Energy for Green Industry at UCLA. The authors would like to thank Professor C S Lynch from UCLA for useful discussions and exchange of information.

References

- [1] Lawrence Livermore National Laboratory 2010 US Energy Flow Trends 2009 <https://publicaffairs.llnl.gov/news/energy/energy.html#2009> September 21

- [2] Olsen R B, Bruno D A, Briscoe J M and Butler W F 1981 A pyroelectric energy converter which employs regeneration *Ferroelectrics* **38** 975–8
- [3] Moran M J and Shapiro H N 2004 *Fundamentals of Engineering Thermodynamics* 5th edn (New York: Wiley)
- [4] Cuadras A, Gasulla M and Ferrari V 2010 Thermal energy harvesting through pyroelectricity *Sensors Actuators A* **158** 132–9
- [5] Fang J, Frederich H and Pilon L 2010 Harvesting nanoscale thermal radiation using pyroelectric materials *ASME J. Heat Transfer* **132** 092701
- [6] Nguyen H, Navid A and Pilon L 2010 Improved pyroelectric energy converter for waste heat energy harvesting using co-polymer P(VDF-TrFE) and Olsen cycle *Appl. Therm. Eng.* **30** 2127–37
- [7] Olsen R B 1982 Ferroelectric conversion of heat to electrical energy—a demonstration *J. Energy* **6** 91–5
- [8] Olsen R B and Brown D D 1982 High-efficiency direct conversion of heat to electrical energy related pyroelectric measurements *Ferroelectrics* **40** 17–27
- [9] Olsen R B, Bruno D A and Briscoe J M 1984 Cascaded pyroelectric energy converter *Ferroelectrics* **59** 205–19
- [10] Hunter S R, Lavrik N V, Bannuru T, Mostafa S, Rajic S and Datskos P G 2011 Development of MEMS based pyroelectric thermal energy harvesters *Proc. SPIE* **8035** 80350V
- [11] Lee F K, Navid A and Pilon L 2011 Pyroelectric waste heat energy harvesting using heat conduction *Appl. Therm. Eng.* **37** 30–7
- [12] Ravindran S K T, Huesgen T, Kroener M and Woias P 2011 A self-sustaining pyroelectric energy harvester utilizing spatial thermal gradients *16th Int. Solid-State Sensors, Actuators and Microsystems Conf. (TRANSDUCERS) (June)* pp 657–60
- [13] Kandilian R, Navid A and Pilon L 2011 Pyroelectric energy harvesting capabilities of PMN-PT near the morphotropic phase boundary *Smart Mater. Struct.* **20** 055020
- [14] Ren W, Liu S-F and Mukherjee B K 2002 Piezoelectric properties and phase transitions of 001-oriented $\text{Pb}(\text{Zn}_{1/3}\text{Nb}_{2/3})\text{O}_3$ - PbTiO_3 single crystals *Appl. Phys. Lett.* **80** 3174–6
- [15] Yin J, Jiang B and Cao W 2000 Elastic, piezoelectric, and dielectric properties of $0.995\text{Pb}(\text{Zn}_{1/2}\text{Nb}_{2/3})\text{O}_3$ - 0.045PbTiO_3 *Trans. Ultrason. Ferroelectr. Freq. Control* **1** 285–91
- [16] Liu S, Park S, Cross L and Shrout R 2002 Temperature dependence of electrostriction in rhombohedral $\text{Pb}(\text{Zn}_{1/3}\text{Nb}_{2/3})\text{O}_3$ - PbTiO_3 single crystals *J. Appl. Phys.* **92** 461–7
- [17] Shen M and Cao W 2007 Investigation of dipolar defects in $(1-x)\text{Pb}(\text{Zn}_{1/3}\text{Nb}_{2/3})\text{O}_3$ - $x\text{PbTiO}_3$ single crystals using different poling methods *J. Appl. Phys.* **101** 014105
- [18] Forrester J S, Kisi E H and Knight K S 2006 Phase transitions in PZN-4.5%PT in the range 4.2–450 K *Physica B* **385/386** 160–2
- [19] Chang W S, Lim L C, Yang P, Moser H O, Wang F T, Tseng C T and Tu C S 2008 Phase transformations in poled PZN-4.5%PT single crystals revealed by combined property measurements and high-resolution diffraction technique *J. Appl. Phys.* **104** 054102
- [20] Lima-Silva J J, Guedes I, Mendes Filho J, Ayala A P, Lente M H, Eiras J A and Garcia D 2004 Phase diagram of the relaxor $(1-x)\text{Pb}(\text{Zn}_{1/3}\text{Nb}_{2/3})\text{O}_3$ - $x\text{PbTiO}_3$ investigated by dielectric and Raman spectroscopies *Solid State Commun.* **131** 111–4
- [21] Davis M, Damjanovic D and Setter N 2006 Temperature dependence of the direct piezoelectric effect in relaxor-ferroelectric single crystals: intrinsic and extrinsic contributions *J. Appl. Phys.* **100** 084103
- [22] Benayad A, Hajjaji A, Guiffard B, Lebrun L and Guyomar D 2007 Electromechanical properties versus polarization and vibration directions of $\text{Pb}[(\text{Zn}_{1/3}\text{Nb}_{2/3})_{0.955}\text{Ti}_{0.045}]\text{O}_3$ single crystals grown by the modified Bridgman method *J. Phys. D: Appl. Phys.* **40** 840–5
- [23] Renault A E, Dammak H, Calvarin G and Gaucher P 2005 Electric-field-induced orthorhombic phase in $\text{Pb}[(\text{Zn}_{1/3}\text{Nb}_{2/3})_{0.955}\text{Ti}_{0.045}]\text{O}_3$ single crystals *J. Appl. Phys.* **97** 044105
- [24] Khodayari A, Pruvost S, Sebald G, Guyomar D and Mohammadi S 2009 Nonlinear pyroelectric energy harvesting from relaxor single crystals *IEEE Trans. Ultrason. Ferroelectr. Freq. Control* **56** 693–9
- [25] Zhu H, Pruvost S, Guyomar D and Khodayari A 2009 Thermal energy harvesting from $\text{Pb}(\text{Zn}_{1/3}\text{Nb}_{2/3})_{0.955}\text{Ti}_{0.045}\text{O}_3$ single crystals phase transitions *J. Appl. Phys.* **106** 124102
- [26] Samara G A 2001 Ferroelectricity revisited—advances in materials and physics *Solid State Physics* vol 56 (San Diego, CA: Academic) pp 239–458
- [27] Kumar P, Sharma S, Thakur O P, Prakash C and Goel T C 2004 Dielectric, piezoelectric and pyroelectric properties of PMN-PT (68:32) system *Ceram. Int.* **30** 585–9
- [28] Li Z, Xi Z, Xu Z and Yao X 2002 Dielectric/ferroelectric response and phase transition of PMN-0.32PT single crystal *J. Mater. Sci. Lett.* **21** 1325–7
- [29] Yasuda N, Banno T, Fujita K, Ohwa H, Matushita M, Yamashita Y, Iwata M and Ishibashi Y 2007 Piezoelectric properties of relaxor ferroelectric solid solution single crystals PMN-PT and PZN-PT near MPB under pressures *Ferroelectrics* **347** 44–9
- [30] Li Z, Xu Z, Xi Z, Xiang F and Yao X 2007 Thermal expansion characteristics in [001]-oriented PMN-0.32PT single crystals *Ferroelectrics* **355** 245–51
- [31] Lines M E and Glass A M 1977 *Principles and Applications of Ferroelectrics and Related Materials* (Oxford: Clarendon)
- [32] Navid A and Pilon L 2011 Pyroelectric energy harvesting using Olsen cycles in purified and porous poly(vinylidene fluoride-trifluoroethylene) thin films *Smart Mater. Struct.* **20** 025012
- [33] Ozgul M 2003 Polarization switching and fatigue anisotropy in relaxor-lead titanate ferroelectric single crystals *PhD Thesis* The Pennsylvania State University
- [34] Liščić B 2009 Heat transfer control during quenching *Mater. Manuf. Process.* **24** 879–86
- [35] Van Randerot J and Setington R E 1974 *Piezoelectric Ceramics* 2nd edn (London: Mullard Ltd)
- [36] Incropera F P, DeWitt D P, Bergman T and Lavine A 2006 *Fundamentals of Heat and Mass Transfer* 6th edn (New York: Wiley)
- [37] Sitti M, Campolo D, Yan J and Fearing R 2001 Development of PZT and PZN-PT based unimorph actuators for micromechanical flapping mechanisms *IEEE Int. Conf. on Robotics and Automation, 2001* pp 21–6
- [38] Fang B, Du Q, Zhou L, Zhao X, Xu H and Luo H 2009 Structural phase transition and physical properties of tetragonal $0.85\text{Pb}(\text{Zn}_{1/3}\text{Nb}_{2/3})\text{O}_3$ - 0.15PbTiO_3 single crystals *J. Appl. Phys.* **106** 074110
- [39] Pandey A, Gottlieb O, Shtempluck O and Buks E 2010 Performance of an AuPd micromechanical resonator as a temperature sensor *Appl. Phys. Lett.* **96** 203105
- [40] Webber K, Hopkinson D and Lynch C 2006 Application of a classical lamination theory model to the design of piezoelectric composite unimorph actuators *J. Intell. Mater. Syst. Struct.* **17** 29–34
- [41] Kumar R, Molin D, Young L and Ke F 2004 New high temperature polymer thin coating for power electronics *Appl. Power Electron. Conf. Exposition* **2** 1247–9